Open Access



RESEARCH ARTICLE

Using water-landing, fixed-wing UAVs and computer vision to assess seabird nutrient subsidy effects on sharks and rays

Melissa Schiele^{1,2} , J. Marcus Rowcliffe¹, Ben Clark², Paul Lepper² & Tom B. Letessier¹

¹Institute of Zoology, Zoological Society of London, London, UK

Keywords

Computer vision, distribution, invasive, sea glitter, sharks, UAV

Correspondence

Melissa Schiele, Institute of Zoology, Zoological Society of London, London, UK. Tel: +44 01509 227645; E-mail: m.schiele@ lboro.ac.uk

Editor: Dr. Temuulen Sankey **Associate Editor**: Dr. Alice Jones

Received: 25 May 2023; Revised: 30 October 2023; Accepted: 6 December 2023

doi: 10.1002/rse2.378

Abstract

Bird colonies on islands sustain elevated productivity and biomass on adjacent reefs, through nutrient subsidies. However, the implications of this localized enhancement on higher and often more mobile trophic levels (such as sharks and rays) are unclear, as spatial trends in mobile fauna are often poorly captured by traditional underwater visual surveys. Here, we explore whether the presence of seabird colonies is associated with enhanced abundances of sharks and rays on adjacent coral reefs. We used a novel long-range water-landing fixed-wing unoccupied aerial vehicle (UAV) to survey the distribution and density of sharks, rays and any additional megafauna, on and around tropical coral islands (n = 14) in the Chagos Archipelago Marine Protected Area. We developed a computer-vision algorithm to distinguish greenery (trees and shrubs), sand and sea glitter from visible ocean to yield accurate marine megafauna density estimation. We detected elevated seabird densities over rat-free islands, with the commonest species, sooty tern, reaching densities of 932 \pm 199 per km⁻² while none were observed over former coconut plantation islands. Elasmobranch density around rat-free islands with seabird colonies was 6.7 times higher than around islands without seabird colonies (1.3 \pm 0.63 vs. 0.2 \pm SE 0.1 per km²). Our results are evidence that shark and ray distribution is sensitive to natural and localized nutrient subsidies. Correcting for non-sampled regions of images increased estimated elasmobranch density by 14%, and our openly accessible computer vision algorithm makes this correction easy to implement to generate shark and ray and other wildlife densities from any aerial imagery. The water-landing fixed-wing long-range UAV technology used in this study may provide cost effective monitoring opportunities in remote ocean locations.

Introduction

Understanding the relationships between sharks and rays and their habitats is key to making informed decisions in marine conservation. Reef sharks and rays, occupy important meso-and apex trophic levels, and fill important ecological roles, including controlling prey distribution and acting as nutrient vectors (Schmitz et al., 2010; Roff et al., 2016) meaning they provide critical functions within marine ecosystems (Letessier et al., 2022; Williams et al., 2018). Shark and ray numbers have declined globally with over 30% of the 470 species listed as 'near-threatened' to 'critically endangered' by the IUCN

(IUCN Red List, 2020), primarily due to unsustainable fishing practices. Their conservation is further complicated by conservative life history strategies, and often greater mobility (Andrzejaczek et al., 2022; Tickler et al., 2017). In addition, challenges in sampling mobile species make it difficult to identify effective conservation measures (Dwyer et al., 2020). It is therefore important to uncover associations and patterns between sharks and rays and their habitat use, to inform conservation strategies and delineate marine protected areas (MPAs).

Seabirds which forage at sea are a key link in the cycle of redistributing nutrients in islands and coastal

²Wolfson School of Engineering, Loughborough University, Loughborough, UK

environments (Signa et al., 2021). Productivity and nutrients from the open ocean are captured through foraging and are transferred onto land through guano deposition. This connectivity has been studied worldwide, including in the Pacific, the Indian Ocean, the Southern Ocean and the Arctic and Mediterranean, revealing increased nitrogen levels in terrestrial and marine organisms proximal to bird populations; evidence for the pronounced effects wildlife has on environments (Anderson & Polis, 1999; Graham et al., 2018; Hentati-Sundberg et al., 2020; Lorrain et al., 2017; McCauley et al., 2012; Michelutti et al., 2009; Otero et al., 2018; Shatova et al., 2016). Recently, studies have demonstrated enhanced growth of herbivorous fishes, macroalgae and sponges on tropical coral reefs adjacent to the islands with bird colonies (Graham et al., 2018). These subsidised reefs may have a greater capacity to recover following coral bleaching, making seabird conservation and coral reef fishery management directly linked (Benkwitt et al., 2019), since coral reef health can be promoted through seabird recolonization following invasive species eradication programs (Benkwitt et al., 2021).

It remains unclear whether localized gradients in productivity influence the distribution of sharks and nonfilter feeding rays. Sharks and rays are sufficiently mobile behaviourally respond to fine-scale patchiness (<10 km) in prey availability and nutrient subsidies (Kiszka et al., 2016; Mourier et al., 2016), leading to highly variable distribution and aggregative behaviour (Bonnin et al., 2019). At the scale of the Indo-Pacific, the geographical area of the Chagos Archipelago (also known as the British Indian Ocean Territories 'BIOT' in polity) harbours elevated shark abundances (Letessier et al., 2019). At finer scales, shark distribution on coral reefs and seamounts appears associated with prey availability (Tickler et al., 2017) and pelagic nutrient advection (Hosegood et al., 2019; Letessier et al., 2016). However, it remains unclear whether nutrient subsidies from seabird colonies on islands may drive shark distribution. Here, we take advantage of an existing contrast in seabirdderived nutrient subsidies, between islands where humans were historically present and islands that remain nearpristine. Islands where humans were present were used as monoculture coconut plantations and most native broadleaf trees there were felled, as a result (Carr, 2011; Graham et al., 2018). These plantation islands are now infested with rats, which predate on tree saplings, chicks and eggs, having a detrimental effect on seabirds, both in the Chagos Archipelago and elsewhere (Borrelle et al., 2015; Hilton & Cuthbert, 2010).

Unoccupied aerial vehicles give ecologists opportunities to gather aerial data on sharks (Butcher et al., 2021) and on islands which are often difficult to land boats on, such

as the islands surveyed in this study. Our UAV was chosen for its endurance and water-landing capabilities, meaning complex landing equipment such as slings or hooks were not necessary (Hodgson et al., 2017).

However, UAV flights are often restricted to early morning and late afternoon to avoid the reflection of the sun on the sea surface (sea glints) known collectively as sea glitter (Casella et al., 2016; Ellis et al., 2020; Kay et al., 2009). Sea glitter can render parts of UAV or satellite images taken over the sea unusable, as they obscure the water below (Kanjir et al., 2018). Sea glitter is therefore an undesirable variable that can influence how many animals can be detected. Aerial imagery is always likely to contain some sea glitter, and – for coastal surveys – land cover, and it is therefore important to account for these elements when accurately measuring survey effort for marine species.

Sea glitter in UAV imagery has previously been quantified subjectively into categorized bands of percentage coverage (Hodgson et al., 2013), but quantifying this coverage manually is time-consuming. Depending on the research question or weighting given to sea glitter, it can sometimes be ignored during analysis (Cornet & Joyce, 2021). Most efforts to correct or account for glitter appear in remote sensing literature (Muller-Karger et al., 2018).

Sea glints can be corrected within multiband satellite imagery using polarization imaging techniques combined with correcting algorithms (Liang et al., 2019; Singh & Shanmugam, 2014) using the near-infrared (NIR) channel (Kay et al., 2009; Lyzenga et al., 2006). In addition, methods to remove sea glitter in multispectral UAV images for benthic and coral classification models have been explored (Muslim et al., 2019). However, a method is lacking for simply quantifying sea glitter, as well as land (trees/shrubs), and exposed sand within red, green and blue (RGB) images, with the purpose of quantifying the area effectively surveyed.

Here we explore spatial patterns in sharks and rays around tropical islands with and without seabirds (ratfree and former plantation), using a novel water-landing fixed-wing UAV. We use opportunistic and systematic surveys over marine and terrestrial habitats, to (1) explore sharks and rays and report other megafauna associated with islands and coral reefs of the Chagos archipelago, (2) determine whether there is an association between seabird colony presence and the abundance of sharks and rays, (3) infer the influence of terrestrial nutrient subsidies on shark and ray distribution and conservation and (4) develop a simple and reproducible computer-vision algorithm and methodology for delineating trees, sand and sea glitter, to quantify ocean area sampled in marine aerial imagery. Finally, we comment of the broader

applications of the water-landing fixed-wing UAV in conservation as a viable tool for data gathering in challenging remote marine environments.

Materials and Methods

Study area

Our study was conducted in the Chagos Archipelago (6°00′ S 71°30′ E) in May 2018 and February 2020. The area was declared a 644 000 km² marine protected area (MPA) in 2010 and is presently the largest no-take area in the Indian Ocean. The Chagos Archipelago has around 55 islands within its isolated archipelago, the largest being Diego Garcia at 44 km² which is the only inhabited island. The lack of human presence means the atolls are often considered "near pristine". Twenty-six of the islands (91.4% of the archipelago's total landmass) had invasive rats (*Rattus rattus*) while 29 were rat-free at the time of sampling, with ten islands designated as Important Bird and Biodiversity Areas (IBAs) (Carr et al., 2020).

Aerial transects and UAV design

We surveyed sharks and rays on the islands and the adjacent coral reef crests and flats, using a custom-made water-

landing fixed-wing UAV. Marine ecological UAV surveys are usually completed using off the shelf multirotor systems which are vulnerable to salt and water corrosion. Additionally, the battery can quickly become depleted in strong winds or squalls, cutting short flights and making landings challenging. Our UAV with a larger payload capacity (takeoff weight ~4.5 kg), facilitates heavier, energy dense batteries at ~570 g each, for sustained flights at 55 kph over long distances, with the ability to better tolerate high wind gusts and squalls. The UAV was adapted for water-landing from a model ordinarily used for terrestrial surveying (Aeromao Amphibious Talon, built in 2019) for the purposes of this research. The UAV was hand-launched, from the research vessel or from the island beaches. The bespoke system has a two-meter wingspan and lands on the sea, for easy retrieval (Fig. 1).

Survey images in 2018 were captured at nadir, with a 12 MP camera (Garmin VIRB) with a polarized lens, set to record an image every second, while a forward-facing live-link surveillance camera (RunCam 2, 1080p), allowed for a live video stream to the ground control station. The UAV underwent engineering improvements between the two expeditions and the nadir camera was changed to the SONY RX0 (1" sensor 15 MP).

A pixhawk cube 2 autopilot and Ardu Pilot Mission Planner (Osborne, 2019) flight control software were used

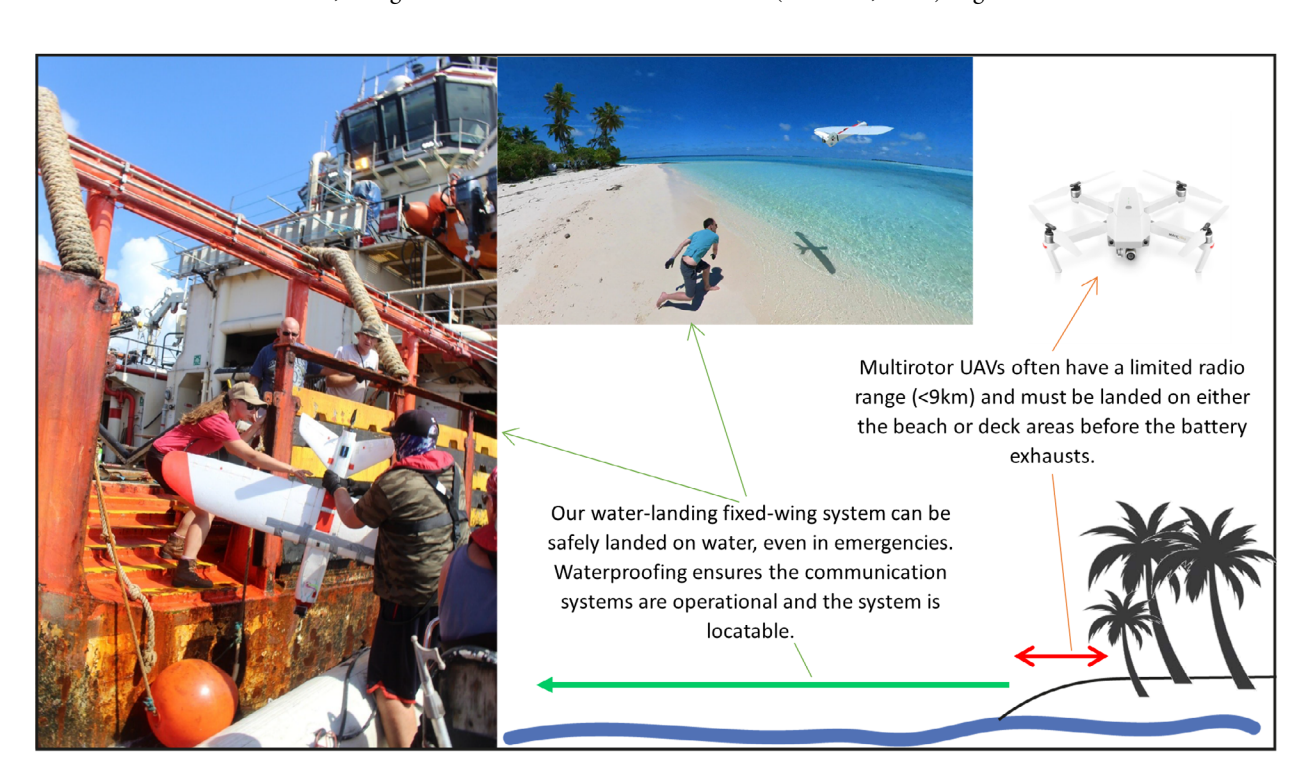


Figure 1. The UAV system is handed back to the pilot by the daughter craft crew, after retrieval from a successful water landing, in 2018. We outline how limited landing opportunities are for multirotor UAVs on many small islands, and in emergencies, this can jeopardise system safety if there is an accidental water landing. Photograph courtesy of Three Wise Monkeys production company and Oceans Unmanned.

ions.onlinelibrary.wiley.com/doi/10.1002/rse2.378 by University College London UCL Library Services, Wiley Online Library on [03/05/2024]. See the Terms

for rules of use; OA articles are governed by the applicable Creative Commons

for piloting the UAV, in fully automatic and semi-manual modes (semi-manual can allow for altitude and speed to be maintained but the pilot can control direction). We opted to fly at 65 m altitude in 2018 and 100 m in 2020. A trade-off exists between achieving meaningful and safe aerial coverage whilst ensuring sufficient resolution to detect wildlife and ensuring similar ground resolution existed between the two expeditions. Our choice of altitudes also reflect efforts to minimize wildlife disturbance (Brisson-Curadeau et al., 2017).

In 2018, intermittent poor weather (high winds >15 knots) meant flights were largely opportunistic, resulting in a sub-optimal sampling strategy. This resulted in the lagoon and ocean-sided flights being imbalanced. In 2020, challenges with logistics and weather were also encountered, but flights overall followed scheduled routes as planned. On some flights (n=3) in 2020, technical issues with the camera meant that film was recorded instead of still images. For these flights, still frames were extracted at 1 per second interval using Adobe Photoshop (AdobeInc., 2023). All flights

were conducted in <20 kph winds, which were recommend for safe and more stable flying, resulting in good visual observation opportunities, thereby limiting variability in visibility and detection of wildlife between sites.

Flights were beyond the visual line of sight (BVLOS) and flight operations were conducted under a permit from the BIOT Administration. Adjacent reefs were surveyed by circumnavigating the islands, to ensure coverage of both the lagoonal and forereef sides in a strip-transect design (Fig. 2). Images produced using this method, do not have decreased perception from the centre to the edges of the images.

Maps were created using QGIS (QGISDevelopment-Team, 2022). Over 15 flights flown (including those not selected for use in our analysis), total distance travelled was 156.9 km and ~15 500 images were gathered. Of this image set, we decided to omit flights from Turtle Cove or the middle of the Great Chagos Bank (GCB), as these areas were either open ocean or did not represent typical rat or non-rat islands (Table 1).

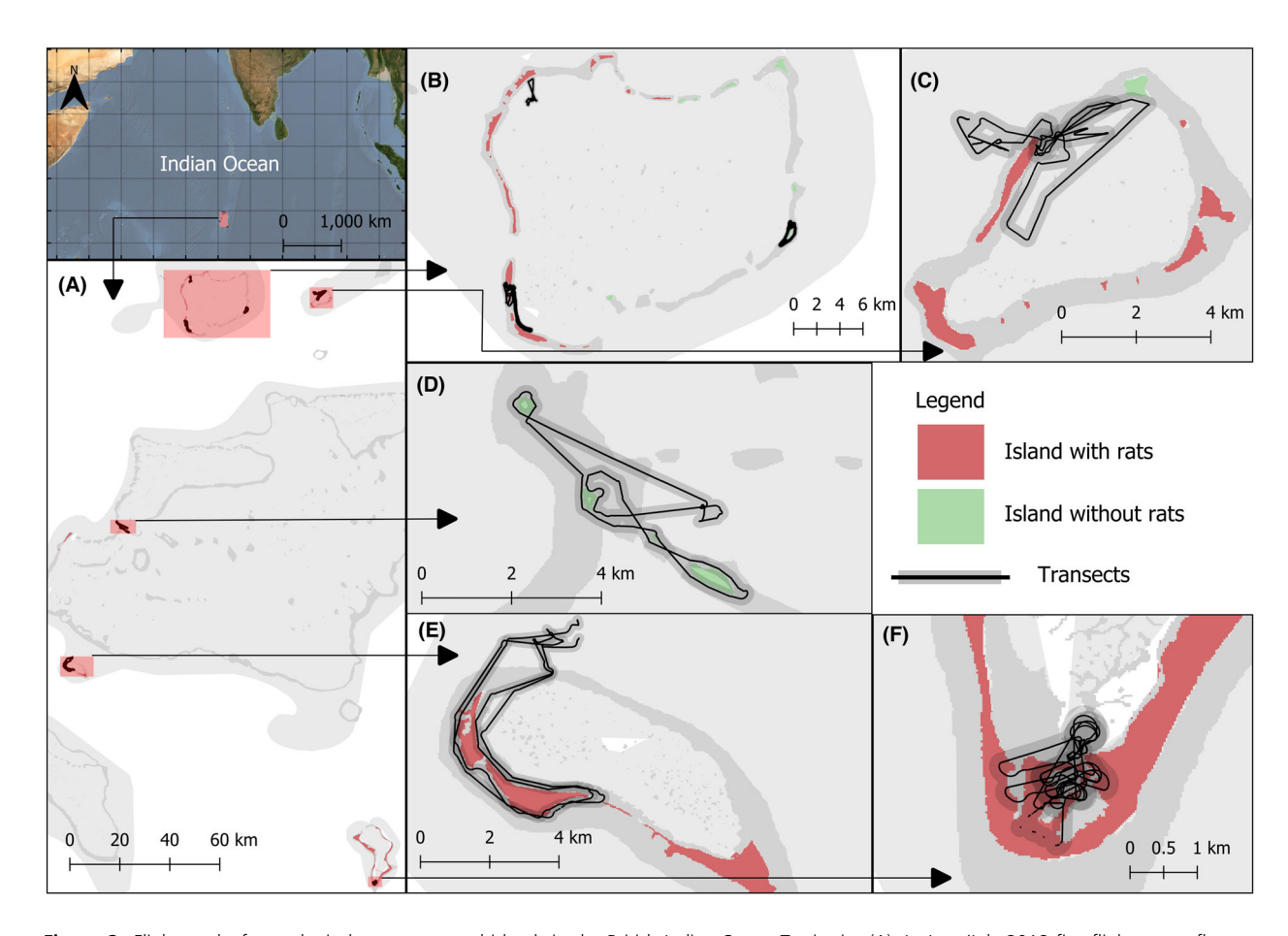


Figure 2. Flight tracks for ecological surveys around islands in the British Indian Ocean Territories (A). In June/July 2018 five flights were flown at Peros Banhos (B) and three at the Salomon islands (C). In February 2020, a single flight was flown at Three Brothers (D), two flights were flown at Egmont (E) part of the Western Great Chagos Banks islands, and three at Turtle Cove in Diego Garcia (F).

TABLE 1. Flights which yielded usable imagery during the 2018 and 2020 expeditions. Flight two's data was lost due to a technical issue. This table reflects the omission of Turtle Cove and GCB images. All flights here are included in the data analysis.

Flight ID	Island		Images after every		% of flight	
		Atoll	5th retained	Distance (km)	Lagoon	Ocean
1	lle Anglaise	Saloman	85	5.8	0	100
3	Ile Anglaise	Saloman	147	8.8	100	0
4	lle Anglaise, lle de la Pas*	Saloman	210	13.7	100	0
5	lle Diamont	Peros Banhos	101	4.5	100	0
6	lle Gabriel, lle Poule	Peros Banhos	265	14.7	35.47	64.53
7	lle Gabriel, lle Poule, lle du Coin, lle Anglaise (PB)	Peros Banhos	237	9.7	100	0
8	Grand Ile Coquillage*	Peros Banhos	224	11.8	44.64	55.36
9	Ile Vache Marine	Peros Banhos	5	0.5	100	0
13	Iles Lubine (Egmont)	Western Islands	190	17.7	72.63	27.37
14	lles Lubine (Egmont)	Western Islands	213	18.2	58.69	41.31
15	North Brother*, Middle Brother*, South Brother*, Resurgence*	Western Islands	297	21.7	39.39	60.61

^{*}Denotes islands without invasive rats.

Wildlife detection

To count wildlife, images were inspected by two independent image analysts. Each image was magnified and inspected, with adjustments to contrast and colour in photoshop where needed, and detections where both observers agreed were retained. A comma-separated values file (CSV) of all images was created, and for each image, the number of detections per taxon was documented, and identified to the lowest taxonomic level possible. To guide identification of birds in UAV imagery, we conducted visits to the islands and visually confirmed the species present. To count large groups of birds which were evenly spaced between individuals, on and around the islands in UAV imagery, we scaled the area occupied by 50–100 birds to the total area sampled by the image.

The frequency of the image capture resulted in overlap in coverage between consecutive images. Exploratory analysis revealed that each individual animal was detected in an average of five consecutive images. We therefore retained every fifth image only, to avoid double counting. This subset of the data frame was used in our models. The original image set was ~15 000 images.

The ground sampling distance (GSD) is measured as cm per pixel. GSD and image area were computed using the PIX4D (Pix4D, 2019) Excel-based utility. GSD for 2018 was 3.67 and 3.57 cm/pixel in 2020.

Quantification and verification of the sea glitter, sand and land delineation method

Many images contained sea glitter, sand and/or land, which needed to be accounted for when calculating the area of

ocean that could potentially yield shark and ray observations. Computer vision techniques (Figure \$1) using RGB colour and greyscale thresholding were developed in MATLAB (MathWorks, 2022), using the built-in Colour Thresholding Application to distinguish unobscured sea from trees, sand and sea glitter in each image. Thresholding is a technique used in image processing to segment an image into different regions based on colour or brightness information (Mery & Pedreschi, 2005). It involves setting a threshold value for each colour channel in an image and then classifying pixels that fall above or below that threshold. In this methodology, manual (by eye) and automated (by MATLAB) masks were created, using values created using manual thresholding. Creating masks manually in the colour thresholding app represents output which is 'as good as we can get it'. However, processing the masks manually for 1975 images would take too long. The purpose of this algorithm is to mask areas of trees, using averaged values of the manual masks, which we consider optimal. It is not always possible to use colour thresholding manually to delineate all the trees in the image, due to variations in foliage colour, some rocks and lighting, which is why the verification of the method is important.

Images were first divided into folders of those which contained land and those which did not. To make the manual colour thresholding more effective, a Gaussian blur was applied to all images, in MATLAB. By averaging the colours of neighbouring pixels, the blur reduces the contrast and sharpness of colours, resulting in a smoother image with less noise.

Manual thresholding was used to delineate trees in 20 images taken from the folder which contains images with land, using the colour thresholder app in MATLAB. For

each image, greenery was represented by min and max values in the red, blue and green channels. The 20 channel values were averaged to give an 'RGB value', which is used in the masking process for the rest of the images. To be included in the mask, pixels must have the same RGB as the averaged value.

The mask values for sea glitter and sand were created using a combination of manual identification of sea glints at pixel level in greyscale images in photoshop (Figure S2) and assessing the histogram distribution (Figure S3) of the greyscale values of these pixels in the

image in MATLAB. For our image set, sea glitter and sand were defined by greyscale pixel values \geq 180 in the 0–255 scale (black to white).

Once the averaged values of trees, sea glitter and sand had been selected, the values were then applied to the whole image set, to create masks (Fig. 3). Both the land mask pixel cover and sea glitter/sand pixel cover were combined, to estimate the percentage of the image that was not usable.

To verify the land and sea glitter/sand identification algorithms, a random sample of 21 images from the

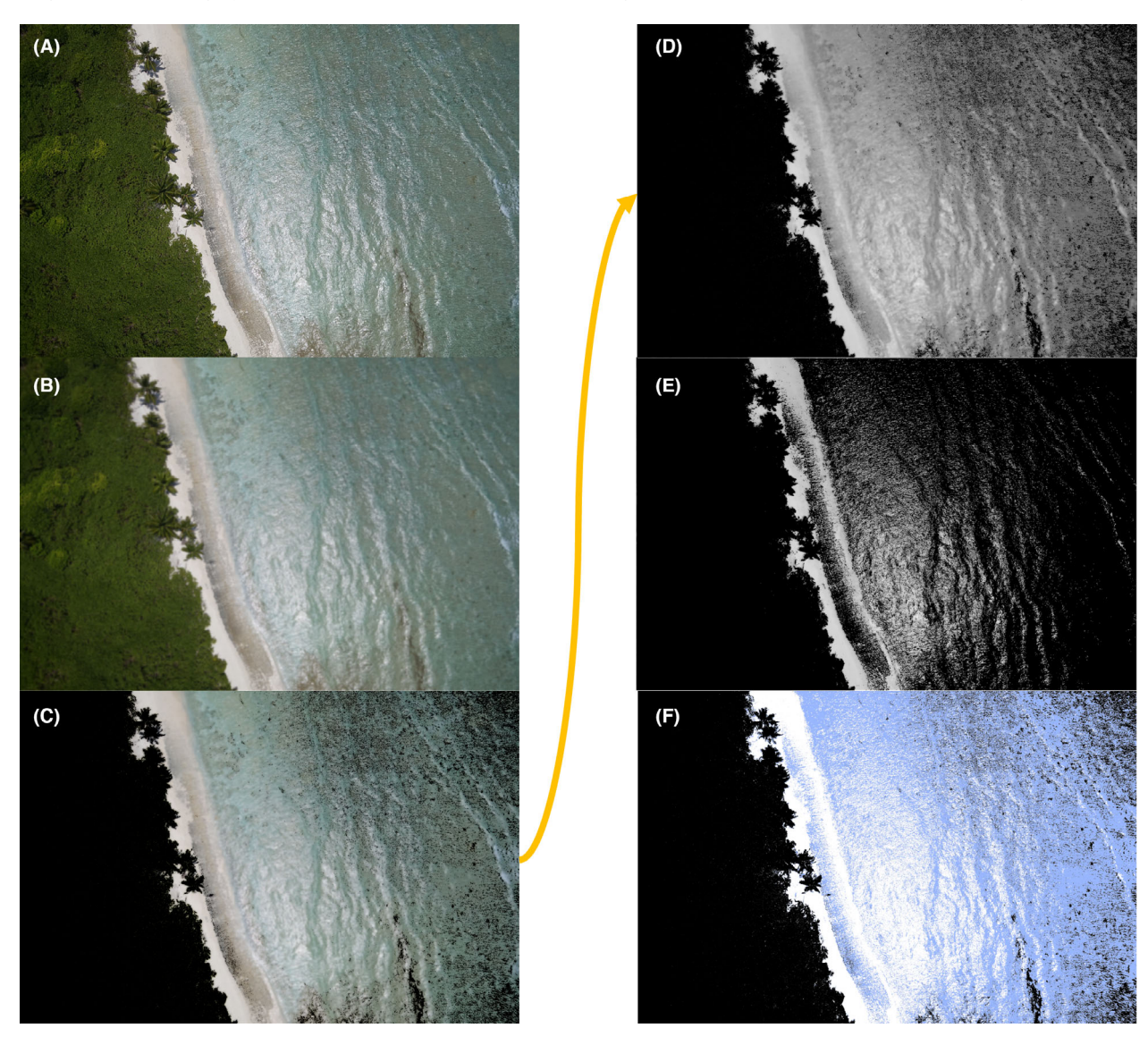


Figure 3. Computer vision steps for batch masking and quantification of trees, sand and sea glitter in the UAV image set. See supplementary information for full workflow. (A) The original image is imported. (B) A Gaussian blur is added. (C) Using the predetermined threshold values, the algorithm computes a mask for the trees (shown in black), additionally, it has masked some areas of the sea incorrectly as trees. (D) The RGB image is converted to greyscale. (E) The sea glitter and sand algorithm computes a mask for sand and sea glitter (shown in white). Pane F is a colourized visual, highlighting the output of the algorithm; the black mask denotes trees, and the white mask denotes sand and sea glitter. The remaining blue is the sampleable sea.

subset containing these features was masked manually in the colour thresholding app in MATLAB and then masked automatically using the algorithm. Disagreement between manual and automated masks was quantified as the percentage of pixels in each image that were classified differently by each method. A linear regression model was used to compare percentages of pixels masked per image between manual and automated methods using R statistical programming (RCoreTeam, 2022) and the difference between mean percentage masking for each method across images was tested using a paired ttest using R package MOTE (Buchanan et al., 2019).

Analysis of faunal abundance

To assess associations between rat presence on islands and the abundance of sharks and rays, we used generalized linear mixed models (GLMM) with Poisson errors, implemented using the R package 'lme4' (Bates et al., 2015) and multi-model inference to evaluate the strength of support for effects.

Flights at Turtle Cove on Diego Garcia were excluded from this analysis because they were targeted at a known immature turtle aggregation (Stokes et al., 2023) area and could not therefore be expected to give a representative picture of turtle distribution in the area. Exploratory analysis of the remaining data revealed that turtle and teleost detections were too spatially aggregated to support robust statistical inference, however, elasmobranch observations were sufficiently dispersed.

The presence/absence of rats and island aspect (lagoon side or oceanside) were tested as the fixed effects in the model of elasmobranch counts, with island identity as a random effect, and the log of area covered multiplied by proportion of pixels without sea glitter/land/sand as an offset. This offset allows us to interpret the model responses as the density of individuals per unit of sea area sampled. We ran a model both with and without the offset to compare its effect on elasmobranch density estimates. Standard errors were bootstrapped by resampling observations with replacement, recalculating densities for each of 100 samples, and taking the standard error of the sampled estimates.

Results

Computer vision verification

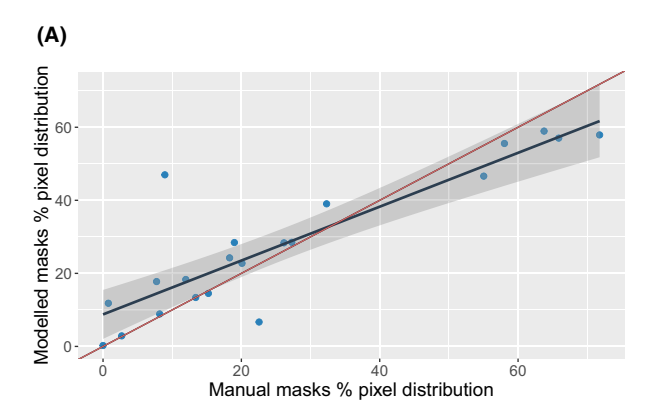
After subsetting the image set of ~15 000, our survey recorded 1976 images, 12.3% of which contained land >1% and 81.83% of images contained sea glitter >1%. Across the 21 images tested for accuracy of the land algorithm, an average of 92.9% of the pixels between the

manually and modelled masks matched. The average percentage of masked pixels was 26.1% in manually processed images, and 28% using the computer vision algorithm. A linear regression of this relationship (Fig. 4A) indicated some overprediction of pixel density at lower values and underprediction at higher values and highlighted one strong outlier with 46.9% mask coverage according to computer vision, compared to 8.9% for the manual mask (48% of pixels classified differently by the methods), though in the same image, sea glitter and sand were manually computed as 13.4% and the modelled mask was 12.9% (2% of pixels classified differently). The outlier was in the flight over the Three Brothers Islands (Fig. 4B). This outlier image (Fig. 4C) proved difficult to mask for sea glitter and trees, both manually and using the model (Fig. 3D). The original image contained deep blue swathes of ocean and rock around the sand. Such deep water is unusual so close to land in our image set. Further examples of images that were more challenging to classify are given in supplements (Figure \$4). Additionally, overexposed images that could not yield wildlife detections, were categorized by the algorithm as sea glitter or sand.

For every 1 pixel increase in the manual mask, the pixels in the modelled mask will increase by 0.7 pixels (95% CI [0.54 to 0.93]). The effect size comparing average per-image mask coverage between methods was negligible (Cohen's d=0.08, 95% CI [-0.71 to 0.53]). No linear relationship was detected between manual and modelled coverage of the sea glitter and sand masks. However, the average percentage coverage of sea glitter and sand was similar between the manual and modelled masks in the test images (10.23 vs. 11.96%), and the two methods disagreed on glitter/sand classification for 11% of pixels.

Faunal distribution and densities

Within the image set, we identified Sooty terns (Onychoprion fuscatus), Red-footed boobies (Sula sula), turtles (Chelonia mydas and Eretmochelys imbricata) and the common Tawny Nurse Shark (Nebrius ferrugineus) (Ferretti et al., 2018) to species level. Noddys (Anous sp.), Frigate birds (Fregata sp.) and other terns could not be identified further than genus level. We identified reef sharks (Carcharhinus sp.), sting rays (Dasyatidae sp.) and eagle rays (Myliobatidae sp.) to genus level and detections of these together with the nurse shark were grouped as 'elasmobranch'. Teleosts (bony fish) were not visually identifiable to genus level. Tropical shearwaters and brown boobies were observed directly but were not detected in UAV imagery. Turtle nesting tracks were detected in UAV images from Egmont, which were



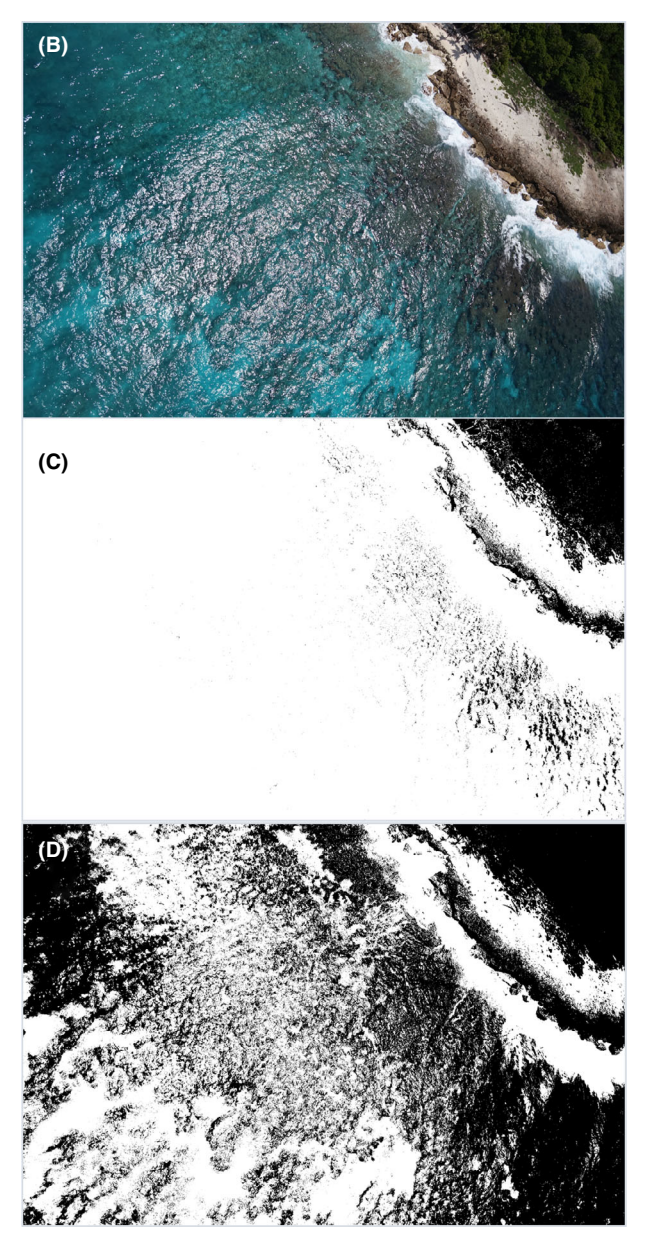


Figure 4. (A) Plot showing relationship between tree cover (%) in survey images using manual and computer vision masking. The positive linear relationship was significant ($r^2 = 0.767$, d.f. = 19, P = 1.957e-07). (B) The outlier image from (A), and the same image manually masked trees (C), and then trees masked by the algorithm (D).

ground-truthed by visiting the island and visually inspecting the nesting tracks. A manta ray (*Mobula* sp.) that we estimated to be around 2 m across, and a whale shark (*Rhincodon typus*) were detected during an opportunistic flight over the Great Chagos Bank, though data from this flight was not used in the final data set in the GLMM. Examples of the detections can be found in supplements (Figure S5).

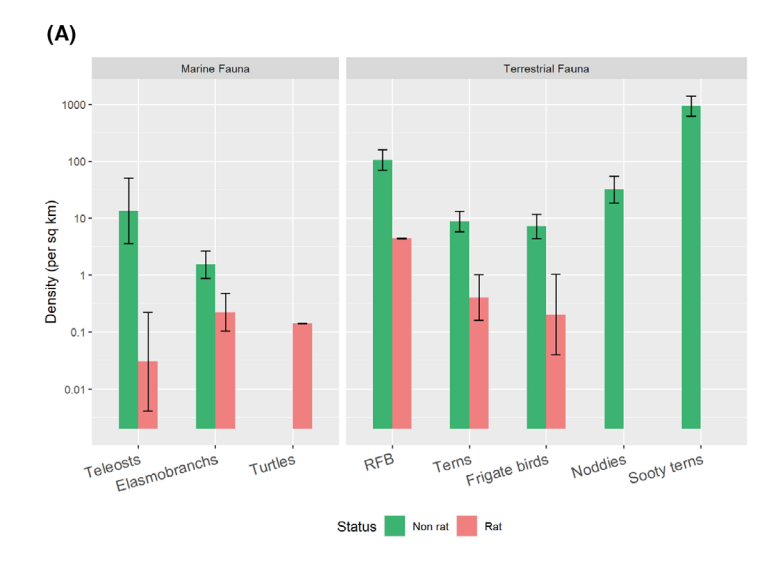
Detections of marine and terrestrial species associated with rat-free islands were higher and more varied than those around rat-infested islands (Fig. 5A). Sooty terns were crowded on nesting sites, reaching densities of 932 ± 199 per km². The Three Brothers flight had a detection of more than one shark in the same image, off-shore from nesting sooty terns on bare ground (Fig. 5B, C). The UAV did not cause any wildlife disturbance as the altitude was sufficient for it to not be viewed as a threat.

The GLMM model of elasmobranch (shark and ray) density as a function of just presence/absence of rats as an explanatory effect had the strongest support, with only weak support for differences between lagoon and ocean side in elasmobranch density (Table 2). Using areas corrected for masking by land and sea glitter, elasmobranch density was 6.7 times higher around rat free islands than around those with rats, with a similar (6.4-fold) difference using uncorrected areas (Fig. 6). Overall, correcting for masking in images increased estimated elasmobranch density by 14%.

Discussion

Overview

Previous studies suggest that rays and sharks are more abundant in nutrient-enhanced areas (Kiszka et al., 2016). We therefore hypothesized that more productive reefs and greater fish biomass levels adjacent to seabird colonies as outlined by Graham *et al.*, may attract more active predatory fishes such as sharks and rays (Graham et al., 2018). Consistent with this hypothesis, we documented elevated numbers of elasmobranchs adjacent to islands without rats, which also had higher nesting seabird abundance. This is consistent with the understanding that nutrient subsidies from productive islands may affect



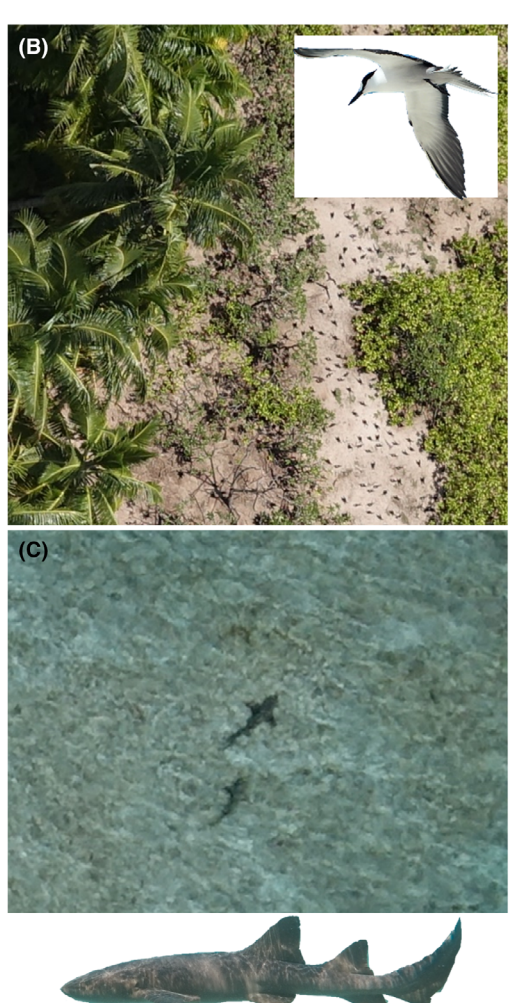


Figure 5. A density bar plot is faceted by marine and terrestrial species, per km². These plots show the densities of each taxon, calculated from the subsetted dataset used in the modelling analysis. The 'old [coconut] plantation' represents rat-infested islands and island without rat are considered near 'pristine'. Although Turtle Cove data was not used, detections of turtles at the Egmont Isles, were retained, as those islands are representative of typical islands in the archipelago. Images from the Middle Brother Island (rat-free) in 2020, highlighting the even spacing of sooty terns in a nesting area (B) and two nurse sharks (C).

TABLE 2. Model selection table for generalized linear mixed models of elasmobranch density as a function of the presence of rats on adjacent islands (Rat) and whether the observation was lagoon or ocean side of the island (Side), with island identity as the random effect.

Model #	Fixed effects structure	d.f.	Log likelihood	AlCc	DAICc	AICc weight
3	Rat Rat+Side	3 4		217.5	0 1.97	0.557 0.208
1	Rat+Side+Rat: Side	5	-104.333	218.7	3.12	0.117
5 4	NULL Side	2	-107.689 -107.570	219.4 221.2	3.80 5.57	0.083 0.034

the distribution of large, marine megafauna species such as sharks and rays (Graham et al., 2018). We did not detect a strong effect of lagoon or ocean sides of islands on elasmobranch densities, which may be due to our opportunistic sampling methods resulting in too few samples to detect any patterns.

Using the novel UAV system, we identified a range of taxa, including sting rays, eagle rays, schooling teleost fishes, nurse and reef sharks, and turtles during UAV flights. We detected a feeding reef manta ray (Mobula alfredi) and a whale shark (Rhincodon typus) alongside the boat at a small sea mount, in the great Chagos bank

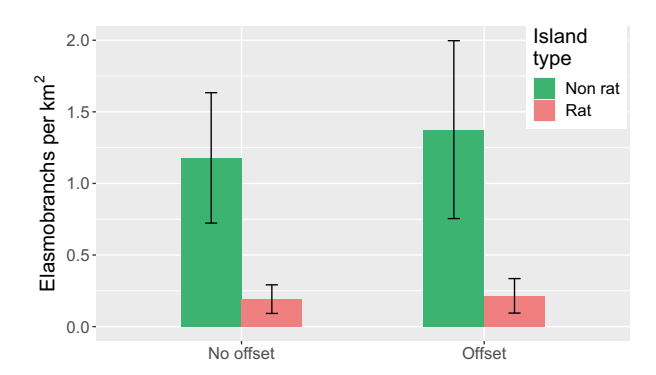


Figure 6. Predicted elasmobranch densities around non-rat and ratinfested islands, either where no correction was included for land and sea glitter coverage (no offset), or where correction was included (offset). Error bars are standard errors.

(though these were not included in the data analyses as they were not associated with islands).

We present evidence suggesting that quantification of sea glitter, trees and sand can affect estimated densities, and that computer vision methods and techniques are replicable. Our study shows that water-landing fixed-wing long-ranged UAVs are suitable tools for gathering ecological data on sharks and rays around remote islands and coral reefs and suggests that they could have wider applications beyond this study in conservation and MPA management.

The use of a computer vision algorithm to automate land/sea delineation

Coastal UAV surveys will often contain unusable areas within some images, and sea glitter is often unavoidable. Area calculations used in any statistical models therefore needed to reflect proportion of unsampleable areas within images (land and sea glitter). Computer vision was chosen as a relatively simple tool for creating an automated, replicable and adaptable, method to attempt batch land and sea glitter quantification. The verification stage of method development sought to test how accurately the thresholding values chosen captured the trees and sea glitter/sand. The linear model for tree masks shows overprediction in the modelled masks at lower pixel densities and underprediction at higher pixel densities in the modelled masks. Images from the data set commonly include the reef area adjacent to islands, which are shallow and agua in colour, and the model can differentiate between the two based on colour. However, when an image contains deep blue areas also containing dark colour green in them, such as around the rocky shores of Middle Brother, or a deep large coral, the model might mask those as trees. The sea glitter/sand mask algorithm though not as accurate as the tree mask algorithm, was still able to produce modelled masks with 89%-pixel similarity. Often, overexposed photos superficially reduced the overall accuracy of the modelled mask. However, an overexposed photo is not likely to yield shark or ray detections. The purpose of the computer vision algorithm is to identify and quantify areas which are unusable for shark and ray detections. Therefore, overexposed areas of images, masked as sea glitter and sand, still technically contribute to unusable parts of the image, albeit as an unintended side-effect.

This method and verification process are easily replicable in MATLAB using the colour thresholding app and some rudimentary scripting (Data S6), and the resulting offset value affected elasmobranch density estimates appreciably. Our image set contained 1975 images, generated from two separate cameras, and at different times of year and day. We attempted to average the heterogeneity within the images to create an effective tool, which can be used as one algorithm on large image sets or split into two if no images contained land: script (1) land (2) sea glitter and/or sand. The script may also be useful if sampleable range of a terrestrial species in a UAV image is stated only as a discrete area of trees, distinct in RGB colour from the surrounding area. We detected a negligible difference in effective pixel coverage between manually masked images compared to modelled masks (Cohen's d = 0.08). We would recommend increasing the initial RGB averaging image set if Cohen's d is medium (\sim 0.5), % values of pixel differences are high (>10%) and if no linear relationship is present when pixel density between the two mask types in the verification image set is plotted. Every UAV image set has unique image composition reflective of the time of day, terrain, sensor type, UAV speed, weather and flight plan. Previously, methods for quantification and removal of sea glitter are mostly associated with satellite remote sensing work (Kay et al., 2009; Lyzenga et al., 2006) with less consideration in dronebased research. Our UAV algorithm compliments other, more complex machine learning algorithms which focus on wildlife detection, by being one which focuses on quantification of habitats to support wildlife density estimates. We therefore present this validated, quick and adaptable computer vision delineation method in place of more complex machine or deep learning algorithms which may require technical expertise, powerful computers and large training data sets (Dujon et al., 2021; Gray et al., 2019; Lassalle et al., 2022).

Surveyed wildlife associated with the islands

We saw consistently low densities of sooty terns, frigate birds and red-footed boobies emerging from the aerial detections, suggesting lower abundance on rat-infested islands. Although brown boobies and tropical shearwaters are known to be present at surveyed atolls and islands (Diego Garcia, Middle Brother, Perhos Banos atoll, Saloman islands and Egmont atoll) (Carr et al., 2020), these species were not detectable in the UAV images. These species are scarce on rat-free islands and absent on rat-infested ones in the case of the brown booby (Hilton & Cuthbert, 2010), or keeping to nests in burrows or sheltered nooks during the day in the case of the shearwater. This behaviour can make them less detectable in UAV-gathered images.

Sooty terns were the most abundant bird, reaching high densities on rat-free islands, nesting with closely packed, equidistant spacing on open ground, where they were easily detectable in UAV imagery. Other birds that nest in dense vegetation (noddies, red-footed boobies) may be less detectable due to screening by foliage. To improve detection rate and hence relative abundance estimates of such species, a thermal infrared (TIR) camera could complement RGB imagery during early morning flights (Whitworth et al., 2022). Flights targeting arboreal birds using the fixed-wing UAV can have altitude reduced to 50 m to attain a usable resolution within the images (GSD ~1.74 cm), though consideration for any wildlife disturbance should be mitigated, by having a tertiary observer documenting animal behaviour. Remote monitoring techniques like this could be especially useful on islands which are difficult to land boats on.

Densities of marine sharks and rays

We found that Nurse sharks are particularly conspicuous in UAV images, but identifying other sharks and rays at species level from UAV imagery can be difficult. In shallow water or when at the surface, we could identify the Tawny Nurse Shark (*Nebrius ferrugineus*) at species level and eagle ray at genus level (*Aetobatus*). It is likely that reef shark species detected are either Silvertip sharks (*Carcharhinus albimarginatus*), Grey reef sharks (*Carcharhinus amblyrhynchos*) or Blacktip reef sharks (*Carcharhinus melanopterus*) (Ferretti et al., 2018; Graham et al., 2010).

Although other comparisons of shark and ray densities between rat and non-rat islands in the Chagos Archipelago are not available, we can compare our results to similar studies from tropical Indo-Pacific reefs. In French Polynesia, UAV flights at 12 m altitude showed elasmobranch densities as high as 93 km⁻² at sites where baiting was used to attract sharks, but much lower at unprovisioned sites (2 km⁻²), and comparable to our density estimates around rate-free islands (1.3 km⁻²) (Kiszka et al., 2016).

However, underwater surveys have given higher densities, with towed-diver surveys in Pacific Island chains yielding reef shark densities from 10.6 to 23 km⁻² (Nadon et al., 2012), and grey reef shark densities estimated using mark recapture methods around Palmyra (considered near pristine) estimated to be 21.3 sharks km² (Bradley et al., 2017). Our lower density estimates may partly or wholly reflect low detectability using aerial surveys in shallow clear waters, emphasizing the need to interpret these numbers as a minimum. However, we have no reason to expect detectability to vary between islands with and without rats in this study, so expect the relative differences in estimated density to reflect a true relative abundance contrast. In deeper water, where variation in time spent at the surface gives greater scope for availability bias, the approach described might still provide a useful signal of relative abundance if methods are applied at consistent locations and under consistent conditions over time, although results need to be treated with caution in this case.

This contrast shows evidence that elasmobranchs are more abundant around islands that host seabird colonies. The effect of rat invasion on island seabird colonies is well-established (Carr et al., 2020; Harper & Bunbury, 2015) and our results are consistent with the hypothesis that this effect has knock-on effects on elasmobranchs (Ferretti et al., 2018). The higher densities of shark and rays around rat-free (or near-pristine) islands is not unique to the Chagos Archipelago but is likely present at other islands where foraging seabirds nest or spend extended periods of time (McCauley et al., 2012). This effect could reflect enhanced overall elasmobranch abundance, however, given that most of the Chagos islands remain rat-infested, and the limited intensity of coverage reported here, it is possible that the enhanced density we observed around rat-free islands simply reflects a redistribution of the existing population, which would be a less positive conservation outcome. Confirming the potential for rat eradication on oceanic islands to enhance overall populations of sharks and rays will require largerscale and long-term monitoring of these populations, a goal that fixed-wing drones could help achieve costeffectively.

The use of water-landing fixed-wing UAVs in ecology and conservation

Our UAV survey methods produced sufficient detections to statistically detect significant differences in elasmobranch densities between habitats, without the need for traditional invasive sampling techniques. Spatial differences in wildlife on islands with and without rats can further support the case for rat eradications in general, and the use of a novel water-landing fixed-wing UAV for this application has wider conservation applications in other MPAs around the world. Long-range water-landing UAVs have both abilities to cover large areas (currently a ~10 km range at 45-55 kph, 1 h+ endurance, in favourable winds not exceeding 20 kph at take-off) and to collect images of a high enough resolution for the detection of sharks and rays as a tool for conservation monitoring. The UAV can be sent to areas which may be deemed too dangerous or expensive to send people, opening new opportunities for data collection and extending our spatial and temporal understanding of other ecological questions. The waterproofed UAV allows for simple landing anywhere on the sea without the need for a large, cleared area of land or complex landing gear on a vessel. The UAV is low-cost (<USD \$3000 to build) in comparison to other fixed-wing systems such as the Scan Eagle (Hodgson et al., 2017) and it uses open-source mission planning software and requires two people to operate it. This makes the system a realistic technology option for the Global South, providing technology acceptance and stakeholder selection are carefully considered (Hubbard et al., 2023).

Future steps towards the further use of a water-landing fixed-wing UAV include detection of illegal, unreported and unregulated (IUU) fishing, which has been identified as one of an increasing threat to regional biodiversity (Collins et al., 2021; Collins et al., 2023). Our UAV system will ultimately include onboard automatic detection algorithms designed to make surveying MPAs and Exclusive Economic Zone (EEZ) borders for illegal fishing vessels more efficient and the system will continue to be developed as a valuable data collection tool for IUU activities (Morton, 2021). We are also applying and adapting established technology adoption and acceptance methods (Hahn et al., 2022; Rezaei et al., 2020; Venkatesh & Bala, 2008) to understand and where possible alleviate barriers to long-term use of this (and other) UAV systems in the hands of local users in the Global South. In the future, this UAV - in combination with our computer vision algorithm for simple delineation and quantification of objects of relevance in the images - provides a set of tools for marine and terrestrial fauna monitoring in remote islands with low barrier to entry.

Acknowledgments

We thank the Bertarelli Foundation and Marine Management Organisation for funding. We are grateful to the Master, chief engineer and crew of the Grampian Frontier for their assistance. We thank the British Indian Oceans Administration (BIOTA) and the Foreign, Commonwealth and Development Office (FCDO) for permissions

granted and field support. We thank Mauricio Ortiz and Aeromao for assistance in the field in 2018 and Steve Lloyd and Dan Ward and the Three Wise Monkeys production company for their assistance in 2020. We thank Professor Nick Graham for leading the expedition in 2018, and for helpful comments on this manuscript. We also thank the Simon Brown and Rhys Diplock from MRAG, and Andy Deary from MMO for support. Finally, we thank the Royal Navy and United States Armed Forces and the United States Merchant Navy, for their enthusiastic support throughout the project.

References

AdobeInc. (2023) Adobe Photoshop.

Anderson, W. & Polis, G. (1999) Nutrient fluxes from water to land: seabirds affect plant nutrient status on Gulf of California. *Oecologia*, **118**, 324–332.

Andrzejaczek, S., Lucas, T.C.D., Goodman, M.C., Hussey, N.E., Armstrong, A.J., Carlisle, A. et al. (2022) Diving into the vertical dimension of elasmobranch movement ecology. *Science Advances*, **8**, eabo1754.

Bates, D., Mächler, M., Bolker, B. & Walker, S. (2015) Fitting linear mixed-effects models using lme4. *Journal of Statistical Software*, **67**(1), 1–48.

Benkwitt, C.E., Gunn, R.L., Le Corre, M., Carr, P. & Graham, N.A.J. (2021) Rat eradication restores nutrient subsidies from seabirds across terrestrial and marine ecosystems. *Current Biology*, **31**, 2704–2711.e4.

Benkwitt, C.E., Wilson, S.K. & Graham, N.A.J. (2019) Seabird nutrient subsidies alter patterns of algal abundance and fish biomass on coral reefs following a bleaching event. *Global Change Biology*, **25**, 2619–2632.

Bonnin, L., Robbins, W.D., Boussarie, G., Kiszka, J.J., Dagorn, L., Mouillot, D. et al. (2019) Repeated long-range migrations of adult males in a common Indo-Pacific reef shark. *Coral Reefs*, 38, 1121–1132.

Borrelle, S.B., Buxton, R.T., Jones, H.P. & Towns, D.R. (2015) A GIS-based decision-making approach for prioritizing seabird management following predator eradication. *Restoration Ecology*, **23**, 580–587.

Bradley, D., Conklin, E., Papastamatiou, Y.P., McCauley, D.J., Pollock, K., Pollock, A. et al. (2017) Resetting predator baselines in coral reef ecosystems. *Scientific Reports*, 7, 43131.

Brisson-Curadeau, E., Bird, D., Burke, C., Fifield, D.A., Pace, P., Sherley, R.B. et al. (2017) Seabird species vary in behavioural response to drone census. *Scientific Reports*, **7**, 17884.

Buchanan, E., G.A., Scofield, J. & Valentine, K. (2019) MOTE: measure of the effect: package to assist in effect size calculations and their confidence intervals.

Butcher, P., Colefax, A., Gorkin, R., Kajiura, S., López, N., Mourier, J. et al. (2021) The drone revolution of shark science: a review. *Drones*, **5**, 8.

- Carr, P. (2011) Important Bird areas the British Indian Ocean Territory. *British Birds*, **104**, 642–659.
- Carr, P., Votier, S., Koldewey, H., Godley, B., Wood, H. & Nicoll, M.A.C. (2020) Status and phenology of breeding seabirds and a review of important Bird and biodiversity areas in the British Indian Ocean Territory. *Bird Conservation International*, **31**, 14–34.
- Casella, E., Collin, A., Harris, D., Ferse, S., Bejarano, S., Parravicini, V. et al. (2016) Mapping coral reefs using consumer-grade drones and structure from motion photogrammetry techniques. *Coral Reefs*, **36**, 269–275.
- Collins, C., Kerry, C., de Vos, A., Karnad, D., Nuno, A. & Letessier, T.B. (2023) Changes in illegal fishing dynamics in a large-scale MPA during COVID-19. *Current Biology*, **33**, R851–R852.
- Collins, C., Nuno, A., Benaragama, A., Broderick, A., Wijesundara, I., Wijetunge, D. et al. (2021) Ocean-scale footprint of a highly mobile fishing fleet: social-ecological drivers of fleet behaviour and evidence of illegal fishing. *People and Nature*, 3, 740–755.
- Cornet, V.J. & Joyce, K.E. (2021) Assessing the potential of remotely-sensed drone spectroscopy to determine live coral cover on heron reef. *Drones*, 5, 29.
- Dujon, A.M., Ierodiaconou, D., Geeson, J.J., Arnould, J.P.Y., Allan, B.M., Katselidis, K.A. et al. (2021) Machine learning to detect marine animals in UAV imagery: effect of morphology, spacing, behaviour and habitat. Remote Sensing in Ecology and Conservation, 7, 341–354.
- Dwyer, R.G., Krueck, N.C., Udyawer, V., Heupel, M.R., Chapman, D., Pratt, H.L., Jr. et al. (2020) Individual and population benefits of marine reserves for reef sharks. *Current Biology*, **30**, 480–489.e5.
- Ellis, S.L., Taylor, M.L., Schiele, M. & Letessier, T.B. (2020) Influence of altitude on tropical marine habitat classification using imagery from fixed-wing, water-landing UAVs. *Remote Sensing in Ecology and Conservation*, 7, 50–63.
- Ferretti, F., Curnick, D., Liu, K., Romanov, E.V. & Block, B.A. (2018) Shark baselines and the conservation role of remote coral reef ecosystems. *Science Advances*, **4**, eaaq0333.
- Graham, N.A.J., Spalding, M.D. & Sheppard, C.R.C. (2010)
 Reef shark declines in remote atolls highlight the need for multi-faceted conservation action. Aquatic Conservation:
 Marine and Freshwater Ecosystems, 20, 543–548.
- Graham, N.A.J., Wilson, S.K., Carr, P., Hoey, A.S., Jennings, S. & MacNeil, M.A. (2018) Seabirds enhance coral reef productivity and functioning in the absence of invasive rats. *Nature*, **559**, 250–253.
- Gray, P.C., Bierlich, K.C., Mantell, S.A., Friedlaender, A.S., Goldbogen, J.A., Johnston, D.W. et al. (2019) Drones and convolutional neural networks facilitate automated and accurate cetacean species identification and photogrammetry. *Methods in Ecology and Evolution*, 10, 1490–1500.

- Hahn, N.R., Bombaci, S.P. & Wittemyer, G. (2022) Identifying conservation technology needs, barriers, and opportunities. *Scientific Reports*, **12**, 4802.
- Harper, G.A. & Bunbury, N. (2015) Invasive rats on tropical islands: their population biology and impacts on native species. *Global Ecology and Conservation*, **3**, 607–627.
- Hentati-Sundberg, J., Raymond, C., Skold, M., Svensson, O., Gustafsson, B. & Bonaglia, S. (2020) Fueling of a marine-terrestrial ecosystem by a major seabird colony. *Scientific Reports*, **10**, 15455.
- Hilton, G.M. & Cuthbert, R.J. (2010) Review article: the catastrophic impact of invasive mammalian predators on birds of the UK overseas territories: a review and synthesis. *IBIS*, **152**, 443–458.
- Hodgson, A., Kelly, N. & Peel, D. (2013) Unmanned aerial vehicles (UAVs) for surveying marine fauna: a dugong case study. *PLoS One*, **8**, e79556.
- Hodgson, A., Peel, D. & Kelly, N. (2017) Unmanned aerial vehicles for surveying marine fauna: assessing detection probability. *Ecology Applied*, 27, 1253–1267.
- Hosegood, P.J., Nimmo-Smith, W.A.M., Proud, R., Adams, K. & Brierley, A.S. (2019) Internal lee waves and baroclinic bores over a tropical seamount shark 'hot-spot'. *Progress in Oceanography*, 172, 34–50.
- Hubbard, E., Schiele, M. & Lepper, P. (2023) Consideration of stakeholders for technology acceptance in marine conservation. Chartered Institute of Ergonomics and Human Factors. Contemporary Ergonomics & Human Factors 2023: Proceedings of the Annual Conference of the Chartered Institute of Ergonomics & Human Factors.
- Kanjir, U., Greidanus, H. & Ostir, K. (2018) Vessel detection and classification from spaceborne optical images: a literature survey. *Remote Sensing of Environment*, **207**, 1–26.
- Kay, S., Hedley, J. & Lavender, S. (2009) Sun glint correction of high and low spatial resolution images of aquatic scenes: a review of methods for visible and near-infrared wavelengths. *Remote Sensing*, 1, 697–730.
- Kiszka, J.J., Mourier, J., Gastrich, K. & Heithaus, M.R. (2016) Using unmanned aerial vehicles (UAVs) to investigate shark and ray densities in a shallow coral lagoon. *Marine Ecology Progress Series*, **560**, 237–242.
- Lassalle, G., de Souza Filho, C.R., Disney, M. & Friess, D. (2022) Tracking canopy gaps in mangroves remotely using deep learning. *Remote Sensing in Ecology and Conservation*, **8**, 890–903.
- Letessier, T.B., Cox, M.J., Meeuwig, J.J., Boersch-Supan, P.H. & Brierley, A.S. (2016) Enhanced pelagic biomass around coral atolls. *Marine Ecology Progress Series*, **546**, 271–276.
- Letessier, T.B., Johnston, J., Delarue, J., Martin, B. & Anderson, R.C. (2022) Spinner dolphin residency in tropical atoll lagoons: diurnal presence, seasonal variability and implications for nutrient dynamics. *Journal of Zoology*, **318**, 10–22.

- Letessier, T.B., Mouillot, D., Bouchet, P.J., Vigliola, L., Fernandes, M.C., Thompson, C. et al. (2019) Remote reefs and seamounts are the last refuges for marine predators across the indo-Pacific. *PLoS Biology*, **17**, e3000366.
- Liang, J.A., Wang, X., He, S. & Jin, W.Q. (2019) Sea surface clutter suppression method based on time-domain polarization characteristics of sun glint. *Optics Express*, 27, 2142–2158.
- Lorrain, A., Houlbreque, F., Benzoni, F., Barjon, L., Tremblay-Boyer, L., Menkes, C. et al. (2017) Seabirds supply nitrogen to reef-building corals on remote Pacific islets. *Scientific Reports*, **7**, 3721.
- Lyzenga, D.R., Malinas, N.P. & Tanis, F.J. (2006) Multispectral bathymetry using a simple physically based algorithm. *IEEE Transactions on Geoscience and Remote Sensing*, **44**, 2251–2259
- MathWorks. (2022) MATLAB: R2022a.
- McCauley, D.J., Desalles, P.A., Young, H.S., Dunbar, R.B., Dirzo, R., Mills, M.M. et al. (2012) From wing to wing: the persistence of long ecological interaction chains in less-disturbed ecosystems. *Scientific Reports*, **2**, 409.
- Mery, D. & Pedreschi, F. (2005) Segmentation of colour food images using a robust algorithm. *Journal of Food Engineering*, **66**, 353–360.
- Michelutti, N., Keatley, B.E., Brimble, S., Blais, J.M., Liu, H., Douglas, M.S. et al. (2009) Seabird-driven shifts in Arctic pond ecosystems. *Proceedings of the Royal Society of London. Series B, Biological Sciences*, **276**, 591–596.
- Morton, K. (2021) Summary of unmanned aerial vehicle trials for use in UK overseas territories 2018–2020 (Marine Management Organisation [Ed.]). UK Government Publishing. https://assets.publishing.service.gov.uk/government/uploads/system/uploads/attachment_data/file/977843/Summary_of_Drone_trial_004_AC.pdf
- Mourier, J., Maynard, J., Parravicini, V., Ballesta, L., Clua, E., Domeier, M.L. et al. (2016) Extreme inverted trophic pyramid of reef sharks supported by spawning groupers. *Current Biology*, **26**, 2011–2016.
- Muller-Karger, F.E., Hestir, E., Ade, C., Turpie, K., Roberts, D.A., Siegel, D. et al. (2018) Satellite sensor requirements for monitoring essential biodiversity variables of coastal ecosystems. *Ecological Applications*, **28**, 749–760.
- Muslim, A.M., Chong, W.S., Safuan, C.D., Khalil, I. & Hossain, M.S. (2019) Coral reef mapping of UAV: a comparison of sun glint correction methods. *Remote Sensing*, 11, 2422.
- Nadon, M.O., Baum, J.K., Williams, I.D., McPherson, J.M., Zgliczynski, B.J., Richards, B.L. et al. (2012) Re-creating missing population baselines for Pacific reef sharks. *Conservation Biology*, 26, 493–503.
- Osborne, M. (2019) ArduPilot Mission Planner.
- Otero, X.L., De La Pena-Lastra, S., Perez-Alberti, A., Ferreira, T.O. & Huerta-Diaz, M.A. (2018) Seabird colonies as

- important global drivers in the nitrogen and phosphorus cycles. *Nature Communications*, **9**, 246.
- Pix4D. (2019) GSD calculator.
- QGISDevelopmentTeam. (2022) QGIS geographic information system. Open Source Geospatial Foundation Project.
- RCoreTeam. (2022) R: a language and environment for statistical computing. Vienna, Austria: R Foundation for Statistical Computing.
- Rezaei, R., Safa, L. & Ganjkhanloo, M.M. (2020)

 Understanding farmers' ecological conservation behavior regarding the use of integrated pest management- an application of the technology acceptance model. *Global Ecology and Conservation*, 22, e00941.
- Roff, G., Doropoulos, C., Rogers, A., Bozec, Y.M., Krueck, N.C., Aurellado, E. et al. (2016) The ecological role of sharks on coral reefs. *Trends in Ecology & Evolution*, **31**, 395–407.
- Schmitz, O.J., Hawlena, D. & Trussell, G.C. (2010) Predator control of ecosystem nutrient dynamics. *Ecology Letters*, **13**, 1199–1209.
- Shatova, O., Wing, S.R., Gault-Ringold, M., Wing, L. & Hoffmann, L.J. (2016) Seabird guano enhances phytoplankton production in the Southern Ocean. Journal of Experimental Marine Biology and Ecology, 483, 74–87.
- Signa, G., Mazzola, A. & Vizzini, S. (2021) Seabird influence on ecological processes in coastal marine ecosystems: an overlooked role? A critical review. *Estuarine, Coastal and Shelf Science*, 250, 107164.
- Singh, R.K. & Shanmugam, P. (2014) A robust method for removal of glint effects from satellite ocean colour imagery. *Open Science Discussions*, 11, 2791–2829.
- Stokes, H.J., Mortimer, J.A., Laloë, J.O., Hays, G.C. & Esteban, N. (2023) Synergistic use of UAV surveys, satellite tracking data, and mark-recapture to estimate abundance of elusive species. *Ecosphere*, 14, e4444.
- Tickler, D.M., Letessier, T.B., Koldewey, H.J. & Meeuwig, J.J. (2017) Drivers of abundance and spatial distribution of reef-associated sharks in an isolated atoll reef system. *PLoS One*, **12**, e0177374.
- Venkatesh, V. & Bala, H. (2008) Technology acceptance model 3 and a research agenda on interventions. *Decision Sciences*, **39**, 273–315.
- Whitworth, A., Pinto, C., Ortiz, J., Flatt, E. & Silman, M. (2022) Flight speed and time of day heavily influence rainforest canopy wildlife counts from drone-mounted thermal camera surveys. *Biodiversity and Conservation*, **31**, 3179–3195.
- Williams, J.J., Papastamatiou, Y.P., Caselle, J.E., Bradley, D. & Jacoby, D.M.P. (2018) Mobile marine predators: an understudied source of nutrients to coral reefs in an unfished atoll. *Proceedings of the Royal Society of London. Series B, Biological Sciences*, **285**, 20172456.

Supporting Information

Additional supporting information may be found online in the Supporting Information section at the end of the article.

Appendix S1. Supporting information.

Figure S1. Complete workflow of the computer vision method for delineating trees, sand and sea glitter.

Figure S2. Sea glints inspection and manual delineation at the pixel level, using Photoshop. The pixel values (between 0 and 255) within the delineation zone were compared to the image pixel histograms created in MATLAB. A range (170–255) was selected which incorporated all glints and sand.

Figure S3. Histograms from greyscale images containing (i) sand and (ii) sea glitter, both with examples from greyscale images. The threshold values of 180–255 encompassed sea glitter and sand pixels. The first large spike in the sea glitter histogram depicts dark areas of sea. Sea glints alone, range from 225 to 255.

Figure S4. Examples of images where the automated algorithm for tree detection either overpredicted (A), predicted accurately (B) or underpredicted mask coverage (C). Figure 6, image (A) shows no greenery. In manual

delineation, as there are no trees, zero pixels were selected manually, however, the algorithm masked the darker blue green of larger corals. Figure 6B shows a 0.9% difference between modelled and manual masks, highlighting an optimal image for the model.

Figure S5. Examples of detections from 2018 to 2020. (A) Turtle at Egmont atoll, (B) Shark in the Saloman islands, (C) Teleosts at Middle Brother island, D() Nurse sharks at Middle Brother island, (E) Shark at Grand Ile Coquillage, (F) Nurse shark at Grand Ile Coquillage, (G) Red footed boobies at Grand Ile Coquillage, (H) Eagle ray at Grand Ile Coquillage, (I) Whale shark at the Great Chagos Bank, (J) Frigate bird at Resurgence island, (K) Turtles at Egmont atoll, (L) Manta ray at the Great Chagos Bank.

Data S1. The script for pulling images into the algorithm, which has the averaged channel values for RGB and sea glitter and sand quantification, using automated masks. Pixel distribution within the sea glitter and sand masks were quantified in MATLAB by using a difference function (utilising the 'Exclusive Or' function) with binary mask inputs $(a-b)^2$, where a = pixels in image one and b = pixels in image two. This function identifies the number of pixels in the two images that are different from each other, which is then expressed as a %.